INL/JOU-17-42045-Revision-0

Modeling Copper Precipitation Hardening and Embrittlement in A Dilute Fe-0.3at.%Cu Alloy Under Neutron Irradiation

Yongfeng Zhang, Benjamin W. Spencer, Xian-Ming Bai, Huibin Ke

November 2017

The INL is a U.S. Department of Energy National Laboratory
operated by Battelle Energy Alliance

INL/JOU-17-42045-Revision-0

Modeling Copper Precipitation Hardening and Embrittlement in A Dilute Fe-0.3at.%Cu Alloy Under Neutron Irradiation

Yongfeng Zhang, Benjamin W. Spencer, Xian-Ming Bai, Huibin Ke

November 2017

Idaho National Laboratory
Idaho Falls, Idaho 83415

http://www.inl.gov

Prepared for the
U.S. Department of Energy

Under DOE Idaho Operations Office
Contract DE-AC07-05ID14517

Modeling Copper Precipitation Hardening and Embrittlement in A Dilute Fe-0.3at.%Cu Alloy Under Neutron Irradiation

Xian-Ming Bai,[1,3*] Huibin Ke,[2] Yongfeng Zhang,[3] Benjamin W. Spencer[3]

[1]Department of Materials Science and Engineering, Virginia Polytechnic Institute and State University, Blacksburg, VA 24061, United States

[2]Department of Materials Science and Engineering, University of Wisconsin – Madison, Madison, WI 53706, United States

[3]Fuel Modeling and Simulation Department, Idaho National Laboratory, Idaho Falls, ID 83415, United States

Abstract:

Neutron irradiation in light water reactors can induce precipitation of nanometer sized Cu clusters in reactor pressure vessel steels. The Cu precipitates impede dislocation gliding, leading to an increase in yield strength (hardening) and an upward shift of ductile-to-brittle transition temperature (embrittlement). In this work, cluster dynamics modeling is used to model the entire Cu precipitation process (nucleation, growth, and coarsening) in a Fe-0.3at.%Cu alloy under neutron irradiation at 300 ˚C. The evolution of the Cu cluster number density and mean radius predicted by the modeling agrees well with experimental data reported in literature for the same alloy under the same irradiation conditions. The predicted precipitation kinetics is used as input for a dispersed barrier hardening model to correlate the microstructural evolution with the radiation hardening and embrittlement in this alloy. The predicted radiation hardening agrees well with the mechanical test results in the literature. Limitations of the model and areas for future improvement are also discussed in this work.

Keywords: Radiation hardening and embrittlement, Reactor pressure vessel steels, Cu precipitation in FeCu alloys, cluster dynamics modeling

*Corresponding author.

Email address: xmbai@vt.edu (X.M. Bai)

I. Introduction

The reactor pressure vessel (RPV) is a safety-critical component in light water reactor nuclear power plants. It contains the reactor core and serves as a physical barrier to prevent the release of radioactive containments to the environment during severe accidents. Because of their massive size and location, RPVs are considered impractical to replace during a reactor's lifetime. In service, RPVs are exposed to long-term neutron irradiation at temperatures around 300°C [1]. For a 40-year service time, typically a RPV receives irradiation dose up to 0.1 displacement per atom (dpa) [1, 2]. As for many other metals and alloys, irradiation can cause an increase of the yield strength (hardening) and a decrease of ductility and fracture toughness (embrittlement) in RPV steels [1, 3]. Due to the radiation hardening and embrittlement, the ductile to brittle transition temperature (DBTT) shifts upward to a higher temperature upon long-term irradiation and thermal aging [1]. It has been shown that the shift in DBTT can be as large as 250°C under some circumstances [1, 4], which could bring the DBTT close to the RPV operating temperature. Even much smaller DBTT shifts can lead to significant increases in the likelihood of a fracture initiating at the location of a pre-existing flaw in an RPV during a transient loading scenario. Therefore, predicting radiation-induced hardening and embrittlement is of significant interest when considering safety implications of long term operation of current reactors.

RPVs are made of iron (Fe) based low-alloy ferritic steels, for which the composition varies slightly for reactors in different countries [1]. Minor elements, including manganese (Mn), nickel (Ni), silicon (Si), etc., as well as copper (Cu), are usually present in RPV steels, either as alloying elements or impurities. The concentration of these minor elements is typically less than 1 wt.%. Although the concentration of minor elements is low, radiation can enhance or induce the precipitation of some alloy elements to form nano-size precipitates [2, 5]. For example, Cu has a very low solubility in body-centered-cubic (bcc) iron. Even at the relatively high temperature of 700°C, the solubility limit is only about 0.5 wt.% [6]. Neutron irradiation in reactors can accelerate the precipitation of Cu through the mechanism of radiation-enhanced precipitation. Other precipitates have also been observed, such as Mn-Ni-Si clusters at high doses (the so-called "Late Blooming Phase") [5, 7]. Although the average size of these clusters is only a few nanometers, they can serve as obstacles for dislocation motion. As a result, the yield strength increases and the failure strain decreases. In addition, irradiation creates dislocation loops and voids in the Fe matrix. These microstructural features also contribute to radiation hardening and embrittlement.

The degradation of the mechanical properties of RPV is directly related to reactor safety and is an important consideration for reactor lifetime extension. In the last few decades, radiation induced precipitation hardening and embrittlement has been an active research area in the nuclear materials field. Many experimental and modeling efforts have been conducted to investigate microstructural evolution and the change in mechanical properties in RPV steels as well as in model alloys. Experimentally, many studies have demonstrated that radiation induced embrittlement in RPV steels is very sensitive to the alloy composition [1]. For example, the increase in the concentration of Cu, Ni, and P leads to an increased susceptibility to embrittlement [1]. It has been shown more recently that Mn content also has a significant impact on embrittlement [8]. At the microstructural level, the properties of precipitates and other defects have been analyzed using a wide range of advanced characterization tools [2] such as small angle neutron scattering (SANS), atom probe tomography (APT), positron annihilation spectroscopy (PAS), and transmission electron microscopy (TEM). Using these advanced microstructural characterization techniques, researchers have obtained valuable information about the composition, radius, number density, and volume fraction of the nanometer-size precipitates in RPV steels and model alloys [1, 2]. The evolution of the precipitates strongly depends on alloy composition and irradiation conditions. Typically,

the volume fraction of the precipitates increases with irradiation dose at low doses then reaches a saturated value at high doses [1]. It should be noted that each characterization technique has limitations, so using a combination of them can provide complementary results for the same sample. In many studies, researchers have demonstrated that Cu-rich precipitates form in RPV steels and model alloys under neutron irradiation. It is commonly accepted that the precipitation of Cu-rich clusters plays an important role in causing radiation hardening and embrittlement in RPV steels. The Fe matrix may also form matrix defect features such as dislocation loops and microvoids [1]. Meslin et al. [2] showed that the number density of dislocation loops is about two orders of magnitude lower than that of Cu precipitates, while the number density of vacancy-type clusters is slightly higher than that of Cu precipitates in Fe-0.1at.%Cu and Fe-0.3at.%Cu model alloys. Lambrecht et al. [9] used a theoretical model to estimate the contribution to radiation hardening from Cu precipitates and matrix defects in these alloys. Their conclusion is that although dislocation loops are stronger obstacles than precipitates for dislocation motion, the contribution from dislocation loops to the hardening is small due to their low number density. Vacancy-type clusters or microvoids are considered to have no contribution to radiation hardening due to their small sizes [9]. The precipitation of other types of clusters such as Mn-Ni-Si clusters at high doses may affect the mechanical properties of RPV steels significantly, and this is a topic of active research [7, 8]. To represent the effect of irradiation on material properties for engineering analyses, models [1] such as the EONY model [4, 8] have been developed to describe the DBTT shift as a function of irradiation doses for RPV steels of different compositions. The parameters in these models are empirically fitted to the database obtained from a large number of the surveillance samples.

Although the engineering models mentioned above are very powerful for predicting the radiation embrittlement of RPV steels, their representation of microstructural evolution is either lacking or based on empirical data rather than physics-based models. Likewise, they employ empirical correlations between microstructure and mechanical properties. In addition, the flux effect [10] is not well addressed in these models, which can be a challenge for extrapolating the results of accelerated irradiation tests to realistic RPV irradiation conditions. Furthermore, the models only can be applied to RPV steels of specific composition ranges [1]. Since the microstructural evolution governs the degradation of the mechanical properties in irradiated RPV steels, mesoscale modeling methods such as kinetic Monte Carlo (KMC) [11-13] and cluster dynamics [14, 15] have been applied to study the Cu precipitation in bcc iron under both irradiation and thermal aging conditions. Becquart and Wirth [12] have used KMC to model Cu precipitation in a Fe-0.3%Cu at dose rates comparable to those experienced by RPV steels in reactors. The cascade-induced defects were introduced into the simulation systems at certain time intervals based on dose rates. One major conclusion from this work is that the decrease in dose rate enhances Cu precipitation. KMC has also been used to study the Cu precipitation in high-Cu Fe-Cu alloys, taking into account the effects of mobile Cu clusters [13]. Although KMC has spatial resolution and can capture some atomic details of the precipitation process, the computational cost is relatively expensive. An alternative approach is rate theory based cluster dynamics modeling [16]. Cluster dynamics is a mean-field approach in which the clusters and defect sinks are assumed to be homogenously distributed in the system. It can model the nucleation, growth, and coarsening of the precipitates in the same framework. The evolution of point defects, which is directly related to radiation-enhanced diffusion of solute atoms, can be naturally coupled to the precipitation model. This method has been successfully applied to model Cu precipitation under electron and neutron irradiation conditions in some high Cu alloys such as Fe-1.34at.%Cu [14] and the predicted precipitation kinetics have good agreement with experimental measurement. In addition to modeling solute precipitation under irradiation [14] and thermal aging [15], this method has also been extensively applied to model the evolution of dislocation loops and voids in pure metals [17, 18].

The Cu concentration in realistic RPV steels is very low, typically below 0.1 at.% [1]. Modeling the Cu precipitation for long irradiation times in these low-Cu alloys is a challenge because of the slow precipitation kinetics in dilute alloys. Moreover, the connection between the size distribution of precipitates and the macro-scale hardening (and embrittlement) has not been well established in low Cu alloys. In this work, we use cluster dynamics modeling to model the Cu precipitation under neutron irradiation conditions at 300 ˚C in a Fe-0.3 at.%Cu alloy, which is much closer to the Cu concentration in realistic RPV steels than the previously studied Fe-1.34 at.%Cu alloys. A size-dependent dispersed barrier hardening model is used to correlate the precipitate size distribution with the radiation hardening and embrittlement. Experimental results for both Cu precipitation kinetics [2] and radiation hardening [9] are available for this alloy in literature, and are used to calibrate our model. Through the combination of cluster dynamics modeling and a dispersed barrier hardening model, the evolution of radiation hardening and DBTT shift as a function of irradiation dose are predicted in this work.

The paper is organized as follows. In Section II, results from the cluster dynamics model for Cu precipitation under election irradiation in a Fe-1.34 at.%Cu [14] are reproduced to ensure the correct implementation of the modeling framework. In Section III, this cluster dynamics model is modified to model Cu precipitation in a Fe-0.3 at.%Cu alloy under neutron irradiation and the results are compared with experiments. In Section IV, a size-dependent dispersed barrier hardening model and a superposition law are used to connect the microstructural evolution with the radiation hardening. In addition, the evolution of DBTT shift as a function of irradiation dose is also predicted based on a correlation between hardening and DBTT shift. Finally discussion and conclusions are presented.

II. Cluster dynamics modeling of Cu precipitation in Fe-1.34 at.%Cu under electron irradiation

Cluster dynamics has been used to model Cu precipitation in bcc Fe under both irradiation [14] and thermal aging [15] conditions. When Cu clusters are small, they have the same bcc crystal structure as the Fe matrix so that the interface between bcc Cu precipitates and Fe matrix is coherent. When the precipitates grow to a certain size (e.g., 2 – 3 nm in radius), the bcc structure transforms to a twinned 9R structure [19-21]. As the precipitate radius grows to about 6 – 10 nm, the crystal structure transforms to a stable face-centered-cubic (fcc) structure [19]. In this work, only the coherent bcc Cu precipitates are modeled because the mean precipitate radius reaches about 2 nm in the dilute Fe-0.3 at.%Cu alloys in experiments [2, 9]. In some previous modeling work, small Cu clusters are considered to be mobile [15]. However, in this work only Cu monomers are considered diffusing, which is the same assumption made in Ref. [14]. Using this simplification, the diffusion of mobile clusters is effectively included in the Cu monomer diffusion.

In this section, the previously published cluster dynamics model for Cu precipitation in a Fe-1.34at.%Cu under electron irradiation [14] is reproduced first to ensure that our cluster dynamics modeling framework works appropriately. Some parameters from this high-Cu model will be adapted to study the Cu precipitation in a dilute Fe-0.3at.%Cu under neutron irradiation, as discussed in the next section. Although the model was described in several references [14, 15, 22], in this manuscript we present the full details of the model to present this approach in a self-contained manner so that other researchers can reproduce this work conveniently. In cluster dynamics modeling, the size of each class of cluster can be represented by the number of atoms it contains. Each class of cluster has a concentration based on the mean field assumption. The concentration of a cluster containing n Cu atoms is represented by C_n. Since only Cu monomers are considered mobile in this work, Cu clusters only interact with single Cu atoms. When a cluster of size n absorbs one Cu monomer, its size become $n+1$. When a cluster of size $n+1$ emits

one Cu monomer through thermal emission, its size decreases to *n*. Therefore, the flux from cluster size *n* to *n+1* is:

$$J_{n\to n+1} = \beta_n C_1 C_n - \alpha_{n+1} C_{n+1}\,, \tag{1}$$

where β_n is the absorption coefficient for a cluster of size *n* and α_{n+1} is the emission coefficient for a cluster of size *n+1*. Assuming all clusters (including monomer) have a spherical geometry, the radius of a cluster of size *n* is $r_n = \left(\frac{3nV_{at}}{4\pi}\right)^{1/3}$, where $V_{at} = a_0^3/2$ is the volume per bcc Cu atom and a_0 is the lattice parameter for bcc Fe. The absorption coefficient β_n is related to the radius of a Cu monomer (r_1), the radius of the Cu cluster of size *n* (r_n), the Cu diffusion coefficient in Fe matrix (D_{Cu}), and the atomic volume of a bcc Cu atom (V_{at}),

$$\beta_n = \frac{4\pi(r_1 + r_n)D_{Cu}}{V_{at}}\,. \tag{2}$$

The emission and absorption coefficients are exponentially related by the binding energy of the Cu cluster (E^b), the Boltzmann constant (k_B), and the temperature (T):

$$\alpha_{n+1} = \beta_n \exp\left(-\frac{E^b_{n+1}}{k_B T}\right). \tag{3}$$

In Eq. (3), the cluster binding energy E^b is size-dependent and related to the cluster interface energy σ. The binding energy for a cluster size of *n+1* is

$$E^b_{n+1} = \Omega - T\cdot\Delta S - (36\pi)^{1/3}\cdot V_{at}^{2/3}\cdot\sigma\cdot[(n+1)^{2/3} - n^{2/3}]\,, \tag{4}$$

where Ω is enthalpy change for dissolving Cu in Fe and ΔS is entropy difference between fcc Cu and bcc Fe, respectively. So $G_1 = \Omega - T\Delta S$ is the Gibbs free energy change for the mixing, which determines the solubility of Cu monomer in Fe at a temperature T:

$$C_{eq}(T) = \exp\left(-\frac{\Omega - T\Delta S}{k_B T}\right). \tag{5}$$

Here Ω/k_B = 6255 K and $\Delta S = 0.866\ k_B$ are used [14], which give the Cu solubility of $C_{eq} = 4.3 \times 10^{-5}$ at 300 ˚C (573 K). Equation (4) can also be viewed as the energy gain associated with attaching a monomer to a cluster of size *n*, or $E_{n+1}{}^b = G_1 + G_n - G_{n+1}$, which is the definition of the binding energy for a cluster of size *n+1*. The interfacial energy is usually treated as a fitting parameter in cluster dynamics modeling [15, 22]. For Cu precipitation in Fe, the value is in the range between 0.15 to 0.5 J/ m^2 for a coherent interface [19]. In some work the interface energy has been treated as both size and temperature dependent [15]. In Ref. [14], the interface energy was not explicitly provided. In our work the interface energy is set to 0.37 J/m^2 regardless of cluster size and temperature. We find that the choice of this interface energy value can reproduce the binding energy in Ref. [14], as shown below. Using Eq. (4), the size-dependent binding energy can be obtained, as shown in Fig. 1. The binding energy increases with the increasing cluster size and gradually approaches to a saturated value. Figure 1 is very similar to the plot of size-dependent binding energy in Ref. [14], indicating that 0.37 J/m^2 is the right value for the interfacial energy.

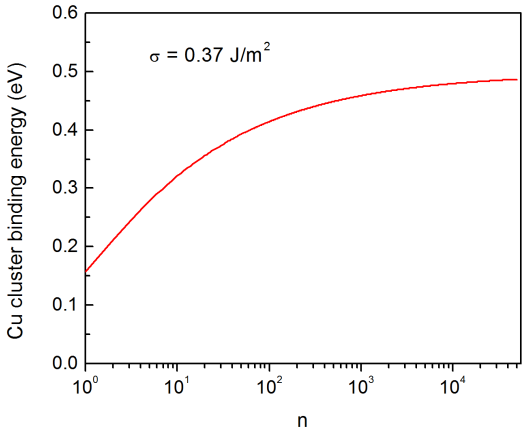

Fig. 1. Size dependence of Cu cluster binding energy.

Since Cu clusters can either grow or shrink, the concentration of each cluster size (C_n) evolves dynamically with time. Each cluster size can evolve to one of its two neighboring cluster sizes through either absorbing or emitting a monomer. Therefore, the time evolution of C_n is related to the fluxes from or to its two neighboring sizes,

$$\frac{dC_n}{dt} = J_{n-1\to n} - J_{n\to n+1}, \qquad (n \geq 2). \tag{6}$$

Note that Eq. (6) is valid only if n ≥ 2 because the flux $J_{0\to 1}$ does not exist. For the evolution of the concentration of the monomer (C_1), the situation is more complex. For all n ≥ 2 fluxes $J_{n\to n+1}$, one Cu monomer is involved through either absorption or emission processes. Therefore, the evolution of C_1 is related to all these n ≥ 2 fluxes. For the flux $J_{1\to 2}$, two Cu monomers are needed to form a di-Cu cluster during the absorption process. Similarly, a di-Cu cluster splits into two Cu monomers during the emission process. So the contribution from the $J_{1\to 2}$ flux to the evolution of C_1 should be doubled. Overall, the time evolution of C_1 can be represented as:

$$\frac{dC_1}{dt} = -2J_{1\to 2} - \sum_{n\geq 2}^{\infty} J_{n\to n+1}\,. \tag{7}$$

Equations (6) and (7) describe the time evolution of all cluster sizes (n = 1 - ∞). Practically, a maximum cluster size n_{max} is used and its flux is set to zero as the boundary condition. Solving the n_{max} ordinary differential equations, the concentration of each cluster size can be obtained as a function of time. Thus the cluster size distribution (i.e., C_n vs. n) also can be obtained at any given time.

Since Cu atoms form substitutional atoms in bcc Fe, the Cu diffusion in Fe is mediated by vacancies during thermal aging. Under irradiation, Cu might also diffuse via the interstitial mechanism. However, Christien and Barbu [14] argued that the contribution from interstitial-mediated Cu diffusion is negligible. Therefore, only the vacancy-mediated Cu diffusion mechanism is considered in this work. For thermal aging, the thermal vacancy concentration determines the Cu diffusivity. Under irradiation, vacancies are produced directly by energetic particles so that the vacancy concentration can be much higher than the

thermal vacancy concentration, particularly at low and moderate temperatures. As a result, Cu diffusion under irradiation is enhanced significantly by irradiation. The radiation enhanced Cu diffusivity is described by

$$D_{Cu}^{irr} = D_{Cu}^{th} \frac{C_v^{irr}}{C_v^{th}}, \quad (8)$$

where the superscripts *th* and *irr* represent the thermal and irradiation conditions, respectively, for vacancy concentration (C_v) and Cu diffusion coefficient (D_{Cu}). The ratio of C_v^{irr} / C_v^{th} is the radiation-enhanced factor for Cu diffusion. The temperature-dependent thermal diffusion coefficient of Cu can be described by $D_{Cu}^{th} = D_{Cu}^0 \cdot \exp(-E_{Cu}^m/k_BT)$, where D_{Cu}^0 and E_{Cu}^m are the prefactor and activation energy of Cu diffusion in bcc Fe, respectively. The thermal vacancy concentration is related to the vacancy formation energy (E_v^f) in Fe and to the temperature by $C_v^{th} = \exp(-E_v^f/k_BT)$. Here $E_v^f = 1.6$ eV is used. The vacancy concentration under irradiation (C_v^{irr}) depends on defect production rate, defect reaction and defect loss to sinks. Here a simplified rate theory model is used to describe the point defect evolution under irradiation. In this model, only defect production, defect recombination, and defect loss to dislocations are considered. For simplicity, defect clustering and other defect sinks are not considered. The time evolution of vacancy concentration (C_v) and interstitial concentration (C_i) are described by the following two rate equations [14],

$$\frac{dC_v}{dt} = \varepsilon G_0 - k_{iv} C_i C_v - z_v D_v C_v \rho_d, \quad (9)$$

$$\frac{dC_i}{dt} = \varepsilon G_0 - k_{iv} C_i C_v - z_i D_i C_i \rho_d, \quad (10)$$

where ε is cascade efficiency; G_0 is defect production rate or irradiation dose rate; k_{iv} is defect recombination coefficient between interstitials and vacancies; $D_v = D_v^0 \cdot \exp(-E_v^m/k_BT)$ is temperature-dependent Fe vacancy diffusion coefficient, where D_v^0 and E_v^m are the prefactor and migration energy for vacancy diffusion, respectively; Similarly, $D_i = D_i^0 \cdot \exp(-E_i^m/k_BT)$ is temperature-dependent Fe interstitial diffusion coefficient, where D_i^0 and E_i^m are the prefactor and migration energy for interstitial diffusion, respectively; ϱ_d is dislocation density; and $z_i = 1.2$ and $z_v = 1.0$ are the dislocation bias factors for interstitials and vacancies, respectively. Typically it is assumed $z_i > z_v$ so that a dislocation absorbs more interstitials than vacancies (the so-called "dislocation bias") [16]. By solving Eqs. (9) and (10), the time evolution of vacancies and interstitials under irradiation can be obtained. This then permits the calculation of radiation enhanced Cu diffusion using Eq. (8).

The cluster dynamics model coupled with radiation-enhanced diffusion model is first used in this study to simulate the precipitation of Cu clusters in a Fe-1.34 at.%Cu alloy under electron irradiation at 290°C with a dose rate of 2×10^{-9} dpa/s, using the same parameters as in Ref. [14]. These parameters are summarized in Table 1. Since electron irradiation only produces Frenkel pairs, the cascade efficiency is ε = 1.0. The dislocation density in the simulation is $\varrho_d = 10^{12}$ m^{-2}. The Fe interstitial and vacancy migration barriers are 0.3 eV and 1.3 eV, respectively. Note that this interstitial migration barrier is close to the atomistic calculation results, but the vacancy migration barrier is about twice of atomistic calculation results for pure Fe [23]. The discrepancy may be attributed to solute or impurity drag effects in realistic alloys. The use of these values in Ref. [14] has resulted in good agreement with experimentally measured precipitation kinetics. Therefore, these migration barriers are used in this study. At the steady state of

point defect evolution, the radiation-enhanced factor for Cu diffusion is about 2.5×10^{7} so that the Cu precipitation kinetics is enhanced significantly by the irradiation. In Ref. [14], Eqs. (9) and (10) were calculated separately from the cluster dynamics modeling and only the steady state value of the radiation-enhanced diffusion factor was used. In our work, Eqs. (9) and (10) are directly coupled to the cluster dynamics modeling [Eqs. (6) and (7)] so that the radiation-enhanced Cu diffusion evolves dynamically during the Cu precipitation process.

Table 1: Parameters for cluster dynamics modeling of Cu precipitation in a Fe-1.34at.%Cu alloy under electron irradiation at 290°C. The parameters are taken from Ref. [14].

Parameter	**Value**
C_1^0, initial Cu concentration	1.34 at.%
a_0, lattice constant of bcc Fe	2.867 Å
T, temperature	563 K (290°C)
E_{Cu}^m, activation energy of Cu thermal diffusion in Fe	2.29 eV
D_{Cu}^0, prefactor of Cu thermal diffusion in Fe	6.3×10^{-5} m^2/s
Ω, heat of mixing of Cu in Fe	6255 k_B·K
ΔS, Entropy of mixing of Cu in Fe	0.866·k_B
σ, interface energy for coherent Cu-Fe interface	0.37 (J/m^2)
G_0, defect production rate	2×10^{-9} dpa/s
ε, cascade efficiency	1.0
ϱ_d, dislocation density	1.0×10^{12} m^{-2}
E_i^m, Fe interstitial migration energy	0.3 eV
D_i^0, prefactor of Fe interstitial diffusion	4.0×10^{-8} m^2/s
E_v^m, Fe vacancy migration energy	1.3 eV
D_v^0, prefactor of Fe vacancy diffusion	1.0×10^{-4} m^2/s
r_{iv}, defect recombination radius	6.5 Å
z_i, dislocation bias factor for interstitials	1.2
z_v, dislocation bias factor for vacancies	1.0
E_v^f, vacancy formation energy in Fe	1.6 eV

The coupled cluster dynamics and rate theory equations ([Eqs. (6-7) and (9-10)]) are solved using the CVODE solver of SUNDIALS package [24]. The Backward Differentiation Formulas (BDF) implicit method is used to integrate the differential equations and Newton method is used for the iteration. At each time step the solver needs to solve $n_{max}+2$ coupled ordinary differential equations. The maximum cluster size n_{max} should be large enough so that the concentration of the largest cluster is close to zero during the entire simulation. However, the computational cost is high when n_{max} is large. To improve the computational efficiency, a few approaches are used. First, a banded linear solver (CVBAND) is used. In this work, only Cu monomers are diffusing. Therefore, for all cluster sizes greater than or equal to 2, C_n only couples with its two neighboring cluster sizes and C_1. As a result, the Jacobian matrix is a banded matrix. The banded linear solver is used to take advantage of this sparse matrix feature. Second, the grouping method developed by Golubov et al. [25] is implemented into our cluster dynamics code. The basic idea of the grouping method is to group clusters into different groups based on their sizes. If the group size is chosen appropriately, the cluster concentration within each group has an approximately linear correlation with the cluster size. Using this method, only two differential equations are solved for each group. The concentration of clusters of each size can then be linearly extrapolated based on the solutions of the two differential equations for a given group. Using the grouping method, the number of

differential equations to be solved can be reduced significantly, with a corresponding improvement in efficiency. To demonstrate that the grouping method works correctly, a test with parameters listed in Table 1 is conducted. In this test, n_{max} = 50,000 and Cu cluster evolution is computed over 50,000 s. For the first 100 cluster sizes, each class of cluster has a group size of 1. For n>100 cluster sizes, the clusters are put into 231 groups so that in total, 331 groups are created. Figure 2(a) compares the evolution of the total Cu cluster number density between the standard cluster dynamics simulation (no grouping) and the grouping method. Here the number density is the number of clusters per unit volume. It can be converted from the cluster concentration by

$$N_n = C_n/V_{at}. \quad (11)$$

In experimental characterization techniques such as small angle neutron scattering (SANS), the detection limit of cluster size (diameter) is about 0.5 – 1.0 nm [2, 9]. Thus using the same definition as in Ref. [14], only clusters containing 10 or more Cu atoms (equivalent to the cluster diameter of 0.6 nm or radius of 0.3 nm) are included in the total cluster number density calculation. Clearly, the grouping method produces results identical to those from the standard method over the entire time range, indicating that the grouping method has been correctly implemented. Figure 2(b) compares the computational times of the two simulations. Using the grouping method, the computational time is reduced by 300 times. In other cases, the computational time has been reduced by up to 400 times.

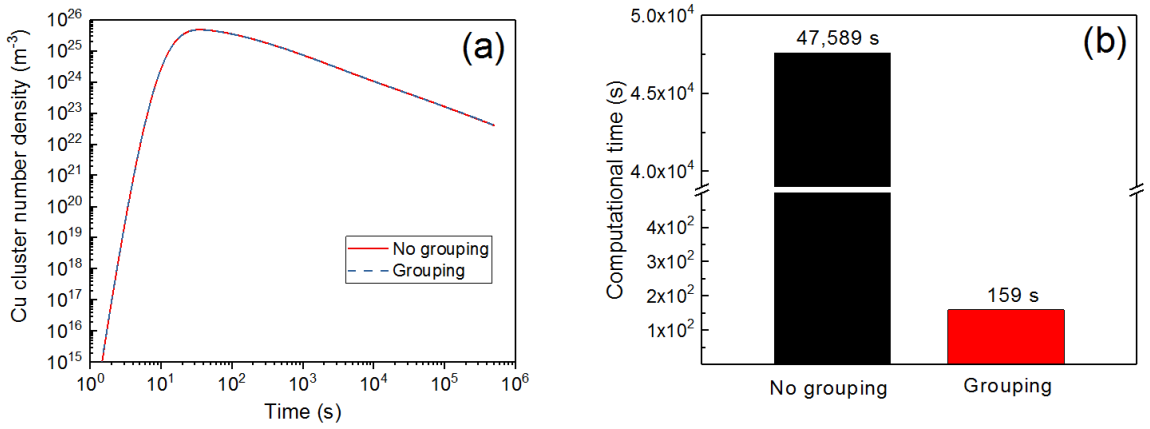

Fig. 2. Comparison of cluster dynamics simulations with and without using the grouping method. (a) The time evolution of the Cu cluster number density. The simulation using grouping method produces results identical to those without using the grouping method. (b) The computational times of the two simulations. The computational time is reduced about 300 times by using the grouping method.

The maximum cluster size (n_{max} = 50,000) used in Fig. 2 is for demonstration purposes only. If the simulation time is long, it was found that this maximum cluster size is not sufficient for studying the Cu precipitation in the Fe-1.34Cu at.% alloy under electron irradiation. Therefore, for the other simulations presented here, a larger maximum cluster size of n_{max} = 200,000 is used. Using the grouping method, 870 groups are created (including the first 100 groups with group size of 1). Precipitate evolution is evaluated over about 2×10^6 s. The solid line in Fig. 3(a) shows the time evolution of the total number density of Cu clusters that contain more than 10 Cu atoms (n>10). The corresponding irradiation dose is also shown in

the top horizontal axis. Similarly, the solid line in Fig. 3(b) shows the time evolution of the mean radius of all the clusters having n>10 Cu atoms. The mean radius is calculated by

$$\bar{r} = \frac{\sum_{n=11}^{n_{max}} (r_n \cdot C_n)}{\sum_{n=11}^{n_{max}} C_n}. \quad (12)$$

As Fig. 3(a) shows, initially the total cluster number density increases rapidly with the irradiation time or dose. Then the number density reaches a maximum value of about 4.5×10^{25} m^{-3} at about 30 s. Meanwhile, the mean cluster radius remains nearly constant. This behavior indicates that the cluster nucleation and growth dominate this stage through depleting the Cu monomers in the Fe matrix. Next the cluster number density decreases but the mean radius increases rapidly. This behavior indicates that the Ostwald ripening induced cluster coarsening dominates the cluster evolution in this regime.

The dose-dependent cluster number densities and mean radii measured from SANS experiments [22] for the same alloy composition under the same electron irradiation conditions are shown as open circles in Fig. 3 for validating the precipitation model. It can be seen that the modeling results agree reasonably well with the SANS experimental results in the coarsening regime for both the total number density of Cu clusters and the mean cluster radius. The results also agree well with published results from the referenced model, indicating that it has been successfully reproduced.

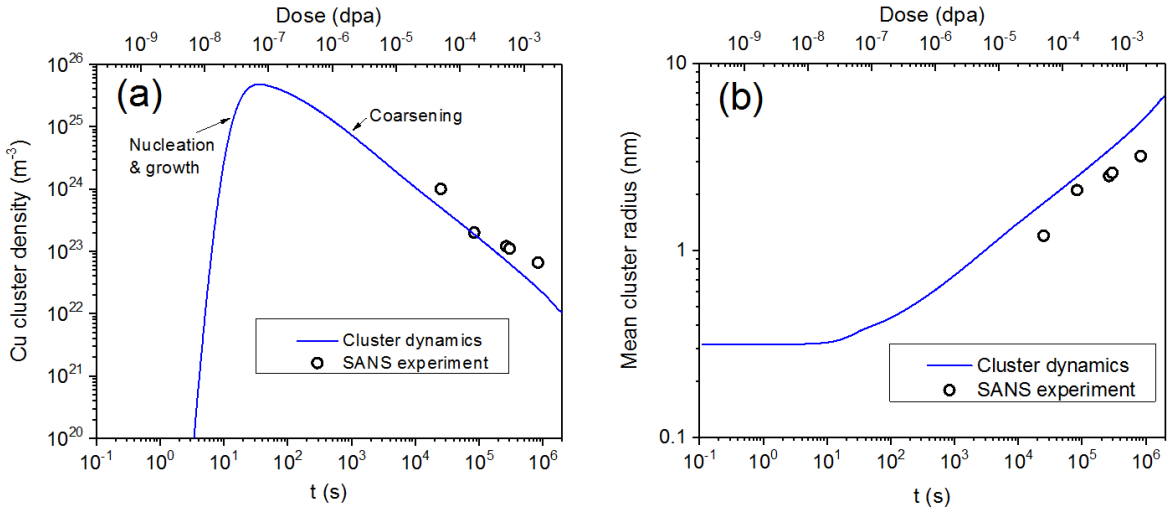

Fig. 3. Cluster dynamics modeling of electron-radiation-enhanced precipitation of Cu clusters in a Fe-1.34 at.%Cu at 290°C based on Ref. [14]. The modeling results (lines) are validated by the small-angle neutron scattering (SANS) experiments (open circles). (a) Evolution of Cu cluster number density as a function of irradiation time or dose. (b) Evolution of the mean Cu cluster radius as a function of irradiation time or dose. Note that in both figures only clusters containing more than 10 Cu atoms are counted.

III. Cluster dynamics model for Cu precipitation in Fe-0.3 at.%Cu under neutron irradiation

In the electron irradiation experiment for the Fe-1.34at.%Cu alloy [22], the Cu concentration is much higher than that in realistic RPV steels, which is typically below 0.1 at.% [1]. When the Cu concentration

is low, precipitation kinetics are also very slow so that longer irradiation times are needed for significant precipitation. Recently, Meslin et al. [2] conducted experimental studies of Cu precipitation in an Fe-based alloy containing 0.3 at.% of Cu under neutron irradiation at 300°C. This Cu concentration is still a little higher than that in realistic RPV steels, but it is much closer than the Fe-1.34Cu at.% alloy. In Meslin et al.'s work, the neutron irradiation dose rate is about 1.4×10^{-7} dpa/s and the dislocation density in the alloy is about $\rho_d = 5\times10^{13}$ m^{-2}. Therefore both the irradiation conditions and material properties are quite different from those in the electron irradiation work.

To test the transferability of the model discussed in Section II, the same parameters listed in Table I (which are for the Fe-1.34Cu at.% alloy under electron irradiation) are first used, except that the material properties (Cu concentration, dislocation density) and irradiation conditions (dose rate, dislocation density, irradiation temperature) are changed to those in the Fe-0.3Cu at.% alloy experiment. Under the new irradiation conditions, the radiation enhanced diffusion factor is 9.1×10^7 at the steady state based on Eqs. (9) and (10). The evolution of the total Cu cluster number density and the evolution of mean Cu cluster radius are shown as the dashed lines in Figs. 4(a) and 4(b), respectively. The results determined by the SANS experiments [2] are shown as the filled circles in each figure. The model as described in Section II predicts lower number density and larger mean radius compared with the experimental results over the entire time range. In other words, the predicted precipitation kinetics from that model are much faster than that in the neutron irradiation experiments. This discrepancy suggests that this model cannot be directly used when the material properties and irradiation conditions change. Therefore, some adjustment of the input parameters is needed.

Although it is very common to adjust the input parameters in cluster dynamics modeling when the material properties and irradiation conditions change, it is desirable to have a model that can predict a variety of conditions with minimal parameter adjustment. In addition, there must be reasonable justification for any adjustment. Here only two parameters are adjusted: the cascade efficiency (ε) and the vacancy migration energy (E_v^m). In the model in Section II, these two parameters have the values: ε=1 and E_v^m=1.3 eV. Recall that that model is for electron irradiation. In electron irradiation, only Frenkel pairs are produced so that defect production efficiency is high ($\varepsilon = 1$). In the Fe-0.3Cu at.% alloy studied here, the Cu precipitation is under neutron irradiation. It is well known that neutron irradiation produces dense collision cascades in which many displaced atoms can have in-cascade recombination. Thus, the defect production efficiency in neutron irradiation is lower than electron irradiation [26]. Similar to the value suggested by Stoller et al. [18], here the cascade efficiency is set to $\varepsilon = 0.4$ to capture the in-cascade recombination effects during neutron irradiation. Using this cascade efficiency, the new results are shown in dotted lines in both figures in Fig. 4. However, this adjustment only slightly improves the agreement of the predicted precipitation kinetics with the experimental results.

Next the vacancy migration energy (E_v^m) is changed from 1.3 eV to 1.0 eV based on the solute drag effect. In alloys, solute elements can interact with point defects and cause solute trapping effects on point defect diffusion. It has been found that Cu atoms and clusters can trap vacancies in Fe [13]. Since in the neutron irradiation experiment the Cu concentration is much lower than in the electron irradiation experiment (0.3 vs. 1.34 at.%), it is reasonable to assume that the effect of solute trapping on vacancy diffusion is weaker in the low-Cu alloy (this work) than in the high-Cu alloy (original model). Therefore, the decrease of the vacancy migration energy from 1.3 eV to 1.0 eV has a reasonable justification although the magnitude of the decrease is empirically chosen. Table 2 summarizes the parameters that are different from those in Table 1. Note that the material properties and irradiation conditions listed in Table 2 are not adjustable parameters because they need be changed to be consistent with the new experiment.

Table 2. Comparison of the parameters for modeling of Cu precipitation in the Fe-1.34at.%Cu and Fe-0.3at.%Cu alloys. Other parameters are as same as in Table 1.

	Original model [14]	**This work**
Materials properties		
C_1^0, initial Cu concentration	1.34 at.%	0.3 at.%
ϱ_d, dislocation density	1.0×10^{12} m^{-2}	5×10^{13} m^{-2}
Irradiation conditions		
Irradiation particles	Electron	Neutron
T, temperature	563 K (290°C)	573 K (300 °C)
G_0, defect production rate	2×10^{-9} dpa/s	1.4×10^{-7} dpa/s
Adjusted parameters		
ε, cascade efficiency	1.0	0.4
E_v^m, Fe vacancy migration energy	1.3 eV	1.0 eV

Using the new cascade efficiency (ε = 0.4) and vacancy migration energy (E_v^m = 1.0 eV), the radiation enhanced Cu diffusion factor decreases from 9.1×10^7 to about 7.7×10^5 at the steady state based on Eqs. (9) and (10). This decrease of Cu diffusion leads to slower coarsening kinetics. The solid lines in Figs. 4(a) and 4(b) show the new cluster dynamics predictions using the new parameter set. The modeling results agree with experimental SANS measurement [2] very well for both cluster number density and mean radius. Compared to the Fe-1.34 at.%Cu alloy under the electron irradiation, the maximum cluster number density is about 20 – 30 times lower because the Cu concentration in the new Fe-0.3 at.%Cu alloy is much lower. The cluster coarsening also happens at a much higher dose range than in the electron irradiation. The mean Cu cluster radius is much smaller for the full range of irradiation doses considered here.

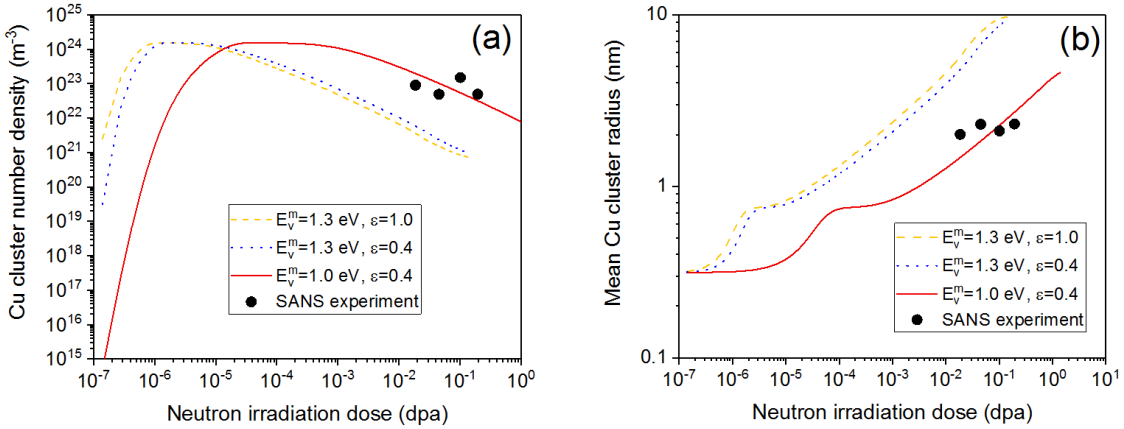

Fig. 4. Cluster dynamics modeling results for neutron-radiation-enhanced precipitation of Cu clusters in a Fe-0.3 at.%Cu at 300°C using three sets of parameters. (a) Evolution of Cu cluster number density as a function of irradiation dose. (b) The evolution of the mean Cu cluster radius as a function of irradiation dose. Note that in both figures only clusters containing more than 10 Cu atoms are counted. In both figures, the dashed lines represent the modeling results using the cascade efficiency (ε = 1.0) and vacancy

migration energy (E_v^m = 1.3 eV) of the model in Ref. [14]. The dotted lines are from changing just the cascade efficiency (ε = 0.4, E_v^m = 1.3 eV). The solid lines represent the final model using two modified parameters (ε = 0.4, E_v^m = 1.0 eV). The results from small-angle neutron scattering experiments (solid circles) [2] are also shown for validation.

At any given irradiation dose (or time), the size distribution of Cu clusters, which is the number density of each class of cluster versus the cluster radius, also can be obtained in addition to the evolution of the total number density and mean cluster radius previously shown. Figure 5 shows the cluster size distribution at 0.14 dpa, which is slightly higher than the upper limit of the total dose received in RPV steels over 40 years [9]. For small clusters (r<0.25 nm), the number density decreases rapidly with the cluster radius. As the cluster radius increases, the number density increases and reaches a maximum value at about r=2.6nm. Beyond that, the number density decreases again with the cluster radius. This size distribution indicates that cluster coarsening takes place at this irradiation dose.

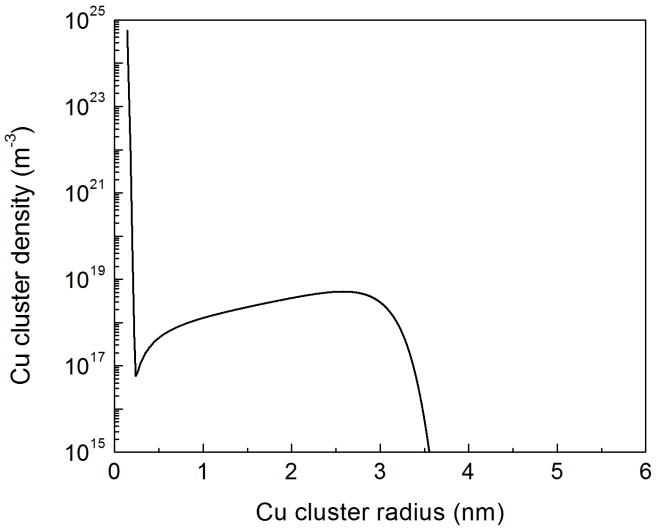

Fig. 5. Cu cluster size distribution at 0.14 dpa in a Fe-0.3 at.%Cu under neutron irradiation at 300°C.

IV. Radiation hardening and embrittlement in Fe-0.3 at.%Cu

In Section III, cluster dynamics predictions of the microstructural evolution during neutron irradiation in the Fe-0.3 at.%Cu alloy were shown. Predicted quantities of interest include the Cu cluster number density, mean cluster radius, and the cluster size distribution. In this section, such microstructural evolution information is connected to the change in mechanical properties such as yield strength. As mentioned earlier, Cu precipitates can become obstacles or pinning points for dislocation motion so that the yield strength of the alloy increases after the irradiation. This is the microscopic origin of radiation-induced precipitation hardening. To make the connection between the precipitates and the hardening, dispersed barrier hardening models such as Orowan's model [27] are widely used. In the conventional Orowan's model, strengthening is achieved through the mechanism of dislocation bowing around spherical precipitates. The increase in the shear strength ($\Delta\tau_s$) is related to the number density (N) and diameter (d) of the precipitates:

$$\Delta\tau_s = \alpha\mu b(Nd)^{0.5} \tag{13}$$

where α is the obstacle or barrier strength with a value between 0 and 1; μ is the shear modulus of the matrix, for which a value of 82 GPa [17] is used for bcc Fe here; b is the Burgers vector of a dislocation, for which a value of $a_0 \cdot \sqrt{3}/2$ is used for the a/2<111> dislocations. Many modifications have been proposed to add more physics to the original Orowan's model. For example, Kelly proposed a modified model [28]:

$$\Delta\tau_s = \alpha \frac{0.83\mu b}{[(Nd)^{-0.5} - d]} \cdot \frac{\ln(d/r_0)}{2\pi(1-\nu)^{0.5}}, \tag{14}$$

Where α, μ, b, N, d have the same meanings as in Eq. (13); r_0 is the dislocation core radius; and ν is the Poisson's ratio. This model has been used by Hu et al. [17] for calculating the radiation hardening induced by dislocation loops and vacancy clusters. In this work this model is used for calculating the hardening induced by Cu clusters. The dislocation core radius is set to r_0=3b (~0.75 nm) and Poisson's ratio is set to ν=1/3. Note in Eq. (14), the cluster diameter should be greater than r_0, d>r_0.

The obstacle strength α depends on the obstacle type, size, and possibly temperature [29, 30]. Typically for the same type of precipitates at the same temperature, the smaller precipitates have less resistance to dislocation motion than larger precipitates [30]. To capture this size-dependent strengthening effect, the empirical equation proposed by Hu et al. [17] is used in this work,

$$\alpha = 1 - \exp\left[-\left(\frac{d}{d_{ref}}\right)^n\right], \tag{15}$$

where the reference cluster diameter d_{ref} = 4 nm and the exponent n=2 are used here. The strength factor α changes from 0 to 1 as the precipitate diameter increases, as shown in Fig. 6.

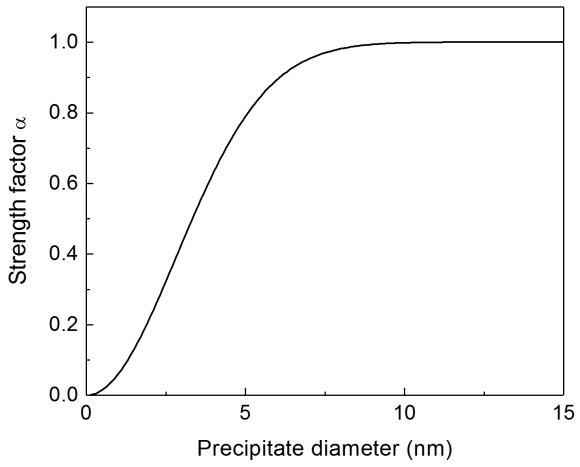

Fig. 6. The strength factor α as a function of Cu precipitate diameter in this work.

The increase in shear strength is correlated to the increase in yield strength by a Taylor's factor M = 3.06 [9],

$$\Delta\sigma_y = M\Delta\tau_s . \quad (16)$$

Table 3. Input parameters for the modified Orowan's equation [Eq. (14-16)].

Parameter	**Value**
μ, shear modulus	82 GPa
ν, Poisson's ratio	1/3
b, Burgers vector	$a_0 \cdot \sqrt{3}/2$
r_0, dislocation core radius	3b
d_{ref}	4.0 nm
n	2.0
M, Taylor's factor	3.06

Therefore, using Eqs. (14) – (16), the increase in the yield strength due to Cu precipitation can be calculated. Some input parameters for these equations are summarized in Table 3. The number density (N) and diameter (d) of the Cu precipitates can be obtained from cluster dynamics modeling as discussed in Section III. Note that here N and d can be treated either for the total set of clusters or individual clusters. Therefore, two approaches are used to calculate the hardening in this work. In the first approach, the total number density of Cu clusters and the average cluster diameter, which are shown in Fig. 4 (note the radius in Fig. 4 should be converted to diameter), are used as N and d to calculate the effective hardening directly. In the second approach, the number density and diameter of each cluster size are used to calculate its individual hardening contribution ($\Delta\sigma_n$). The N and d of each cluster size can be obtained from the cluster size distribution (Fig. 6) at any given time. Once the individual hardening contribution from each cluster size is obtained, the overall hardening can be calculated based on a superposition law. The superposition law can be linear sum, square root of the quadratic sum, or a combination of them [31], although none of them has a clear physical basis. Consistent with Hu et al.'s work [17] for voids and dislocation loops, we also found that the linear sum superposition law overpredicts the strengthening behavior significantly. Therefore in this work the square root of the sum of the squares superposition law is used to predict the total hardening due to all clusters,

$$\Delta\sigma_y = \sqrt{\Delta\sigma_1^2 + \Delta\sigma_2^2 + \Delta\sigma_3^2 + \dots} . \quad (17)$$

Using the two approaches, the evolution of radiation hardening as a function of the irradiation dose can be calculated, as shown in Fig. 7(a). It can be seen that the two approaches give very similar results, suggesting that Eq. (17) works very well in this work. In both approaches, the hardening increases with dose very rapidly at low doses and reaches a saturated value of about 230 MPa at high doses.

Lambrecht et al. [9] have measured the increase in the yield strength at different irradiation doses in a Fe-0.3at.%Cu alloy. However, the measured hardening includes the contribution from both Cu clusters and Fe matrix defect clusters because it is impossible to separate them in experiments. Therefore, for a fair comparison with our modeling work, which only considers the effect of Cu clusters, the contribution from

matrix damage should be deducted. Here a reverse superposition law is applied to extract the net contribution from Cu clusters,

$$\Delta\sigma_{Cu} = \sqrt{\Delta\sigma_{Fe-Cu}^2 - \Delta\sigma_{Fe}^2} \ . \tag{18}$$

In Lambrecht et al.'s work [9], the hardening in a pure Fe was also reported at the same doses as in the Fe-Cu alloy. Therefore the hardening solely due to the Cu cluster precipitation can be calculated using Eq. (18). The experimental data is shown as filled circles in Fig. 7(a). It can be seen that the modeling results agree well with the experimental results.

Based on the analysis of extensive experimental data, Eason et al. [4, 8] found that the ductile-to-brittle transition temperature (DBTT) shift correlates strongly with the increase in yield strength. The relation between them can be approximated as a linear dependence by

$$\Delta T_{DBTT} = 0.71 \cdot \Delta\sigma_y \,, \tag{19}$$

where ΔT_{DBTT} is the change in the ductile-to-brittle transition temperature in degrees C. Based on the hardening evolution calculated from the first approach (i.e., using the total number density and average diameter of all clusters), the evolution of the DBTT shift can be predicted as a function of irradiation dose using Eq. (19), as shown in Fig. 7(b). The DBTT shift increases rapidly at low doses and saturates at about 160 ˚C at high doses.

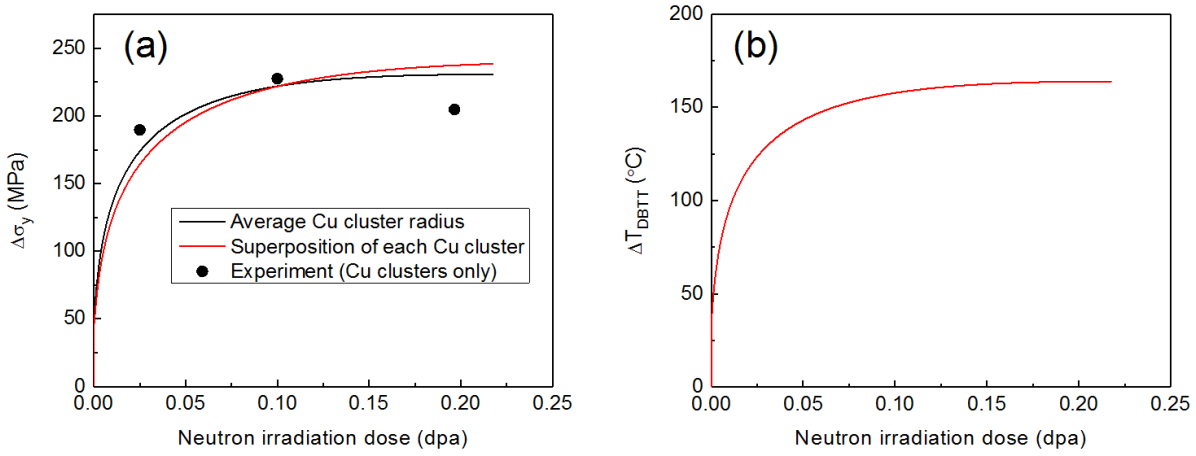

Fig. 7. Evolution of radiation hardening and embrittlement in a Fe-0.3at.%Cu alloy predicted by modeling. (a) Cu-cluster-induced hardening predicted by the modified Orowan model (lines), using the cluster dynamics simulation results as input for the model. The two approaches of calculating the hardening give similar results. Experimental results (filled circles) [9] are also shown for validation. (b) Predicted DBTT shift as a function of irradiation dose.

V. Conclusions and Discussion

In this work, cluster dynamics modeling is used to model Cu cluster precipitation in a dilute Fe-0.3at.%Cu alloy under neutron irradiation at 300 ˚C. The model is adapted from a previously proposed

model for Cu precipitation in a high-Cu alloy (Fe-1.34at.%Cu) under electron irradiation. We modified this model considering two effects: the in-cascade Frenkel pair recombination effect during neutron irradiation and solute trapping effect on vacancy diffusion. The results predicted by our modified model agree well with the precipitation kinetics measured by small angle neutron scattering experiments [2], for both the number density and mean radius of Cu clusters. The characteristics of Cu precipitates (number density, radius, size distribution) predicted by the cluster dynamics modeling are used as input for a modified Orowan's hardening model to predict the evolution of precipitation hardening during neutron irradiation. The size-dependent obstacle strength is included in the hardening model. A superposition law of square root of the quadratic sum is used to account for the contribution from different sized clusters to the overall hardening. The predicted hardening agrees well with the experimental results of the same alloy under the same irradiation conditions in literature. Finally the shift in the ductile-to-brittle transition temperature is predicted for the entire irradiation dose range. The results from this work can be used to understand the precipitation kinetics of Cu-rich clusters and the accompanying radiation hardening and embrittlement in realistic reactor vessel steels which contain dilute Cu. The model may also be adapted to study precipitation hardening induced in other alloys under irradiation or thermal aging conditions.

Our cluster dynamics model is adapted from a literature model that was used to study Cu precipitation in a high-Cu Fe based alloy of distinct materials properties and under different irradiation conditions, as shown in Table 2. However, we showed that only two parameters need to be adjusted and both adjustments can be well justified. This success suggests that the model is relatively robust and it has the potential to predict the Cu precipitation kinetics for other Fe-Cu alloys of different composition and under different irradiation conditions. Despite this initial success, there are still many areas for further improvement of the model. In experiments, it has been found that the Cu precipitates are Cu-rich clusters [32]. However, in our modeling work the clusters are assumed to be pure Cu clusters. The Cu clusters can transform to a 9R structure and the stable fcc structure as the cluster size increases [19-21]. Previous modeling work shows that the inclusion of such phase transformation mechanisms can improve the robustness of the precipitation model [19]. In this work such phase transformation mechanisms are not considered because the mean size of the Cu clusters is small in a dilute alloy. However, inclusion of the phase transformation may make the model to be applicable for a wide range of compositions. Previous kinetic Monte Carlo work [13] shows that small-size Cu clusters may be mobile. In this work, only Cu monomers are assumed to be diffusive and the cluster diffusion is effectively included in the Cu monomer diffusion. However, explicit inclusion of Cu cluster diffusion [15] may improve the robustness of the model. In addition, in this work only homogenous Cu precipitation is considered. In reality heterogeneous precipitation of Cu at preexisting dislocations and irradiation induced defect clusters may also take place, affecting precipitation kinetics [33]. Such heterogeneous precipitation is thermodynamically preferred at various types of defects and has been demonstrated in an earlier work using Metropolis Monte Carlo [34]. This effect may be considered in the future by using cluster dynamics for both radiation damage and solute precipitation.

The vacancy concentration under irradiation, which is directly used to calculate the radiation enhanced copper diffusivity, is obtained from a simple rate theory model. In this model, only defect production, defect recombination, and defect loss to dislocations are considered. The defect clustering effect is not considered. It has been shown that the inclusion of the defect clustering does not affect the late-stage coarsening kinetics, but it slows down the early-stage precipitation kinetics (i.e., nucleation and growth) [14]. Currently the experimental precipitation kinetics data are only available in the late-stage coarsening regime (Figs. 3 and 4). Therefore, experimental data on the early-stage precipitation kinetics can be very helpful for validating the cluster dynamics model. However, the time in this stage is short and reliable

experimental data may not be obtained accurately. Alternatively, other modeling methods such as Kinetic Monte Carlo modeling may provide valuable information in this regime.

The radiation hardening due to Cu precipitates is predicted by a modified Orowan's hardening model. A size-dependent obstacle strengthening factor [Eq. (15)] is used to account for the differing resistance to dislocation motion from various sized precipitates. The reference cluster diameter (d_{ref}) and the exponent (n) in this model are empirically chosen parameters. Molecular dynamics simulations may provide more science-based justification for choosing these parameters. The predicted hardening in this work only includes the contribution from Cu clusters. The matrix defect structures (dislocation loops, voids, etc.) and other types of precipitates (e.g., Mn-Ni-Si) are not included in the current model. To develop more predictive models for predicting the radiation hardening and embrittlement in realistic RPV steels, the contributions from these other types of clusters should also be included in the future.

Acknowledgements

This work is supported by the DOE Office of Nuclear Energy Light Water Reactor Sustainability (LWRS) Program. X.M.B. would like to thank the financial support from Battelle Energy Alliance (Idaho National Laboratory) to Virginia Tech through the Grizzly Project and the Faculty Joint Appointment Program. The authors acknowledge the use of the computing facilities at the High Performance Computing at Idaho National Laboratory and the Advanced Research Computing at Virginia Tech. This manuscript has been co-authored by Battelle Energy Alliance, LLC under Contract No. DE-AC07-05ID14517 with the U.S. Department of Energy. The United States Government retains and the publisher, by accepting the article for publication, acknowledges that the United States Government retains a nonexclusive, paid-up, irrevocable, world-wide license to publish or reproduce the published form of this manuscript, or allow others to do so, for United States Government purposes.

References

[1] C. English, and J. Hyde, *4.05 - Radiation Damage of Reactor Pressure Vessel Steels A2 - Konings, Rudy J.M*, in *Comprehensive Nuclear Materials* (Elsevier, Oxford, 2012), pp. 151.

[2] E. Meslin *et al.*, *Characterization of neutron-irradiated ferritic model alloys and a RPV steel from combined APT, SANS, TEM and PAS analyses*, Journal of Nuclear Materials **406**, 73 (2010).

[3] K. Farrell, T. S. Byun, and N. Hashimoto, *Deformation mode maps for tensile deformation of neutron-irradiated structural alloys*, Journal of Nuclear Materials **335**, 471 (2004).

[4] E. D. Eason, G. R. Odette, R. K. Nanstad, and T. Yamamoto, *A physically-based correlation of irradiation-induced transition temperature shifts for RPV steels*, Journal of Nuclear Materials **433**, 240 (2013).

[5] G. R. Odette, and G. E. Lucas, *Recent progress in understanding reactor pressure vessel steel embrittlement*, Radiation Effects and Defects in Solids **144**, 189 (1998).

[6] G. Salje, and M. Fellerkniepmeier, *DIFFUSION AND SOLUBILITY OF COPPER IN IRON*, Journal of Applied Physics **48**, 1833 (1977).

[7] P. B. Wells *et al.*, *Evolution of manganese–nickel–silicon-dominated phases in highly irradiated reactor pressure vessel steels*, Acta Materialia **80**, 205 (2014).

[8] E. D. Eason, G. R. Odette, R. K. Nanstad, and S. Yamamoto, *A Physically Based Correlation of Irradiation-Induced Transition Temperature Shifts for RPV Steels*, Oak Ridge Report ORNL/TM-2006/530 (2007).

[9] M. Lambrecht *et al.*, *On the correlation between irradiation-induced microstructural features and the hardening of reactor pressure vessel steels*, Journal of Nuclear Materials **406**, 84 (2010).

[10] G. R. Odette, T. Yamamoto, and D. Klingensmith, *On the effect of dose rate on irradiation hardening of RPV steels*, Philosophical Magazine **85**, 779 (2005).

[11] F. Soisson *et al.*, *Atomistic Kinetic Monte Carlo studies of microchemical evolutions driven by diffusion processes under irradiation*, Journal of Nuclear Materials **406**, 55 (2010).

[12] C. S. Becquart, and B. D. Wirth, *1.14 - Kinetic Monte Carlo Simulations of Irradiation Effects*, in *Comprehensive Nuclear Materials*, edited by R. J. M. Konings (Elsevier, Oxford, 2012), pp. 393.

[13] F. Soisson, and C. C. Fu, *Cu-precipitation kinetics in alpha-Fe from atomistic simulations: Vacancy-trapping effects and Cu-cluster mobility*, Physical Review B **76**, 214102 (2007).

[14] F. Christien, and A. Barbu, *Modelling of copper precipitation in iron during thermal aging and irradiation*, Journal of Nuclear Materials **324**, 90 (2004).

[15] T. Jourdan, F. Soisson, E. Clouet, and A. Barbu, *Influence of cluster mobility on Cu precipitation in α-Fe: A cluster dynamics modeling*, Acta Materialia **58**, 3400 (2010).

[16] S. I. Golubov, A. V. Barashev, and R. E. Stoller, *Radiation Damage Theory*, in *Comprehensive Nuclear Materials*, edited by R. J. M. Konings (Elsevier, Oxford, 2012), pp. 357.

[17] X. Hu, D. Xu, T. S. Byun, and B. D. Wirth, *Modeling of irradiation hardening of iron after low-dose and low-temperature neutron irradiation*, Modelling and Simulation in Materials Science and Engineering **22**, 065002 (2014).

[18] R. E. Stoller, S. I. Golubov, C. Domain, and C. S. Becquart, *Mean field rate theory and object kinetic Monte Carlo: A comparison of kinetic models*, Journal of Nuclear Materials **382**, 77 (2008).

[19] G. Stechauner, and E. Kozeschnik, *Thermo-kinetic modeling of Cu precipitation in α-Fe*, Acta Materialia **100**, 135 (2015).

[20] P. J. Othen, M. L. Jenkins, G. D. W. Smith, and W. J. Phythian, *Transmission electron microscope investigations of the structure of copper precipitates in thermally-aged Fe—Cu and Fe—Cu—Ni*, Philosophical Magazine Letters **64**, 383 (1991).

[21] P. J. Othen, M. L. Jenkins, and G. D. W. Smith, *High-resolution electron microscopy studies of the structure of Cu precipitates in α-Fe*, Philosophical Magazine A **70**, 1 (1994).

[22] M. H. Mathon *et al.*, *Experimental study and modelling of copper precipitation under electron irradiation in dilute FeCu binary alloys*, Journal of Nuclear Materials **245**, 224 (1997).

[23] L. Malerba *et al.*, *Comparison of empirical interatomic potentials for iron applied to radiation damage studies*, Journal of Nuclear Materials **406**, 19 (2010).

[24] https://computation.llnl.gov/projects/sundials.

[25] S. I. Golubov, A. M. Ovcharenko, A. V. Barashev, and B. N. Singh, *Grouping method for the approximate solution of a kinetic equation describing the evolution of point-defect clusters*, Philosophical Magazine A **81**, 643 (2001).

[26] G. S. Was, and T. Allen, *Radiation-induced segregation in multicomponent alloys: Effect of particle type*, Materials Characterization **32**, 239 (1994).

[27] E. Orowan, *Symposium on Internal Stresses in Metals and Alloys* (Institute of Metals, 1948).

[28] P. M. Kelly, *Progress Report on Recent Advances in Physical Metallurgy: (C) The Quantitative Relationship between Microstructure and Properties in Two-Phase Alloys*, International Metallurgical Reviews **18**, 31 (1973).

[29] P. M. Rice, and S. J. Zinkle, *Temperature dependence of the radiation damage microstructure in V–4Cr–4Ti neutron irradiated to low dose*, Journal of Nuclear Materials **258–263, Part 2**, 1414 (1998).

[30] D. J. Bacon, Y. N. Osetsky, and D. Rodney, *Chapter 88 Dislocation–Obstacle Interactions at the Atomic Level*, in *Dislocations in Solids*, edited by J. P. Hirth, and L. Kubin (Elsevier, 2009), pp. 1.

[31] G. R. Odette, G. E. Lucas, G. Tedeski, and B. D. Wirth, *DEVELOPMENT OF SUPERPOSITION RULES FOR HARDENING IN ALLOYS CONTAINING MULTIPLE DEFECT POPULATIONS*, Fusion Materials Semiannual Progress Report for Period Ending **25 (DOE/ER-0313/25)**, 221 (1998).

[32] R. Prakash Kolli, and D. N. Seidman, *The temporal evolution of the decomposition of a concentrated multicomponent Fe–Cu-based steel*, Acta Materialia **56**, 2073 (2008).

[33] B. Radiguet, A. Barbu, and P. Pareige, *Understanding of copper precipitation under electron or ion irradiations in FeCu0.1 wt% ferritic alloy by combination of experiments and modelling*, Journal of Nuclear Materials **360**, 104 (2007).

[34] Y. Zhang *et al*., *Preferential Cu precipitation at extended defects in bcc Fe: An atomistic study*, Computational Materials Science **101**, 181 (2015).